Title	Electrochemical formation of ordered pore arrays in InP in KCl
Authors	Quill, Nathan;Lynich, Robert P.;O'Dwyer, Colm;Buckley, D. Noel
Publication date	2012-03-15
Original Citation	Quill, N., Lynch, R. P., O'Dwyer, C. and Buckley, D. N. (2012) 'Electrochemical formation of ordered pore arrays in InP in KCl', ECS Transactions 50(6), pp. 377-392. http://ecst.ecsdl.org/content/50/6/377.abstract
Type of publication	Article (peer-reviewed)
Link to publisher's version	http://ecst.ecsdl.org/content/50/6 - 10.1149/05006.0377ecst
Rights	© The Electrochemical Society
Download date	2024-04-19 18:30:50
Item downloaded from	https://hdl.handle.net/10468/2829

Electrochemical Formation of Ordered Pore Arrays in InP in KCl

N. Quill, R. P. Lynch, C. O'Dwyer[†], D. N. Buckley

Department of Physics and Energy, University of Limerick, Limerick Ireland
Materials and Surf. Sci. Institute, University of Limerick, Limerick Ireland
[†] Present address: *Department of Chemistry, University College Cork, Cork Ireland and Micro & Nanoelectronics Centre, Tyndall National Institute, Lee Maltings, Cork, Ireland*

Pores are formed electrochemically in n-InP in KCl electrolytes with concentrations of 2 mol dm^{-3} or greater. The pore morphology is similar to what is seen in other halide-based electrolytes. At low potentials, crystallographically oriented (CO) pores are formed. At higher potentials, current-line oriented (CLO) pores are formed. Crystallographically oriented pore walls are observed for both pore morphologies. When formed at a constant current, potential oscillations are observed which have been correlated to oscillations in the pore width. The CLO pore wall smoothness and overall uniformity increase as KCl concentration is increased. The porous structures formed in KCl compare favourably with those formed in the more acidic or alkaline electrolytes that are typically used to form these structures.

Introduction

The anodic formation of porosity in semiconductors has received considerable attention, both for the prospect of elucidating the fundamental mechanisms of semiconductor etching and for the wide range of possible applications of porous semiconductors and porous materials in general (1-8). A variety of different porous structures can be obtained by varying electrolyte type and concentration (9-10), substrate type (11), orientation (12) and doping density (13). While much of the work has focused on porous silicon (1, 7), a wide range of porous structures have also been formed in III-V compounds (5-6, 8, 14). In InP, two distinct pore morphologies can be identified, CO pores (8, 15-16) and CLO pores (17-18). CO pores typically form at lower potentials whereas CLO pores typically form at higher potentials. These structures are typically formed in highly acidic electrolytes such as HCl (18) or highly alkaline electrolytes such as KOH (8), while very few studies have examined pore formation in neutral electrolytes (14). Here we show pore formation in a neutral pH KCl electrolyte for the first time. It will be shown that it can reproduce many of the features of porous layers formed in other electrolytes. These pores show a high degree of uniformity relative to their counterparts formed in acidic or alkaline electrolytes. This is evidenced by the observation of smooth, crystallographically bounded pore walls which cannot be produced in the standard HCl electrolyte without the use of additives (19). The high degree of order that is observed, allows for the possibility of fabricating ordered photonic crystals, Bragg reflectors or waveguide structures. This can be achieved by modulating the bulk refractive index of the structure by periodically switching between the lower porosity CO structure and the higher porosity CLO structure (20-21). Combining these properties with the ability to selectively form these structures

at pre-patterned sites on the electrode surface (22) allows for the fabrication of a wide range of complex, tailored structures. The fact that this high degree of order can be obtained in a safer, neutral-pH electrolyte, makes KCl an exciting new electrolyte for the formation of porous InP.

Experimental

The working electrode consisted of polished (100)-oriented monocrystalline sulphur doped ($n = 5 - 5.6 \times 10^{18}$ cm^{-3}) n-InP. An ohmic contact was made to the back of the InP electrode and the back and sides of the electrode were isolated electrically from the electrolyte by means of a suitable varnish. The electrode area was typically 0.2 cm^2. The etch pit density of all samples used was less than 5×10^3 cm^{-2}. Anodization was carried out in aqueous 4 mol dm^{-3} KCl electrolytes unless otherwise stated. A conventional three-electrode cell configuration was used employing a platinum counter electrode and a saturated calomel reference electrode (SCE) to which all potentials were referenced. Prior to immersion in the electrolyte, the working electrode was dipped in an etchant (3:1:1 H_2SO_4:H_2O_2:H_2O) for 4 minutes and then rinsed in deionised water. All electrochemical experiments were carried out in the absence of light. The temperature was held at 25°C by a thermostatic water bath connected to a water jacket cell in which the experiments were carried out.

A CH Instruments Model 650A Electrochemical Workstation was employed for cell parameter control and for data acquisition. Cleaved {011} cross-sections and the (100) surface were examined using a Hitachi S-4800 field emission scanning electron microscope (SEM) operating at 5 kV.

Results and Discussion

Porous layer formed by Linear Potential Sweep (LPS) in 4 mol dm^{-3} KCl

Figure 1 shows a linear sweep voltammogram (LSV) of n-InP in 4 mol dm^{-3} KCl. The potential of the sample was swept form 0 to 3.3 V at 25 mV s^{-1}. SEM examination of the sample shows that the increase in current density seen at potentials greater than 1 V is due to the formation of a porous layer on the electrode surface.

The complete porous layer, which extends ~33 μm into the sample, is shown in Fig. 2 (a). Figure 2 (b) shows a higher magnification image of the region of the porous layer near the electrode surface. Crystallographic pore growth is observed and typical pore widths in this region are between 30 – 50 nm. The pores appear to have a triangular cross section with crystallographically bounded pore walls. Figure 2 (c) is an image of the layer at a depth of around 14 μm. The pores in this image clearly deviate from their preferential crystallographic orientation and align themselves in the direction of current flow. The pores still regularly attempt to branch out along preferential crystallographic directions and typical pore widths remain between 30 and 50 nm.
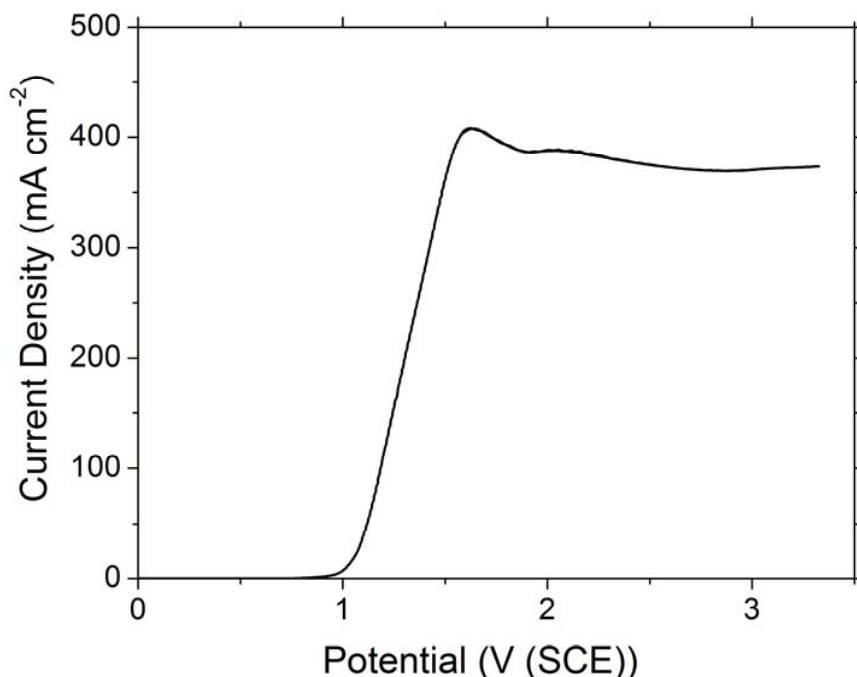
Figure 1. LSV of an InP electrode subjected to a potential sweep from 0 to 3.3 V at a sweep rate of 25 mV s^{-1} at in 4 mol dm^{-3} KCl.

Figure 2 (d) is a higher magnification image of the region of the porous layer near the interface between porous and bulk InP. Here, fully current-line oriented (CLO) pores are observed. The pore width varies significantly in this region but the average value has increased to approximately 70 nm. The inter-pore spacing has become very narrow in this region indicating an overall increase in porosity as the pore morphology switches from CO to CLO. The values of potential and current for pore formation, as well as the pore morphologies observed are similar to what is seen for pore formation in other halide-based electrolytes (14, 18, 23).

Potentiostatic Etching of Porous Layers in KCl

The formation of porous layers in KCl at a constant applied potential was also investigated. Figure 3 shows a series of current-time plots for samples anodized at a range of constant potentials. The sample anodized at 1.0 V shows a gradual increase in current indicative of a progressive nucleation of porous etching sites on the electrode surface, and the gradual expansion of porous domains beneath the surface. This is followed by a plateau in current for the duration of the anodization. The samples anodized at 2.0 V and 3.0 V both show an initially large value of current which decays continuously in time, indicative of an instantaneous nucleation of porous etching across the entire electrode surface.
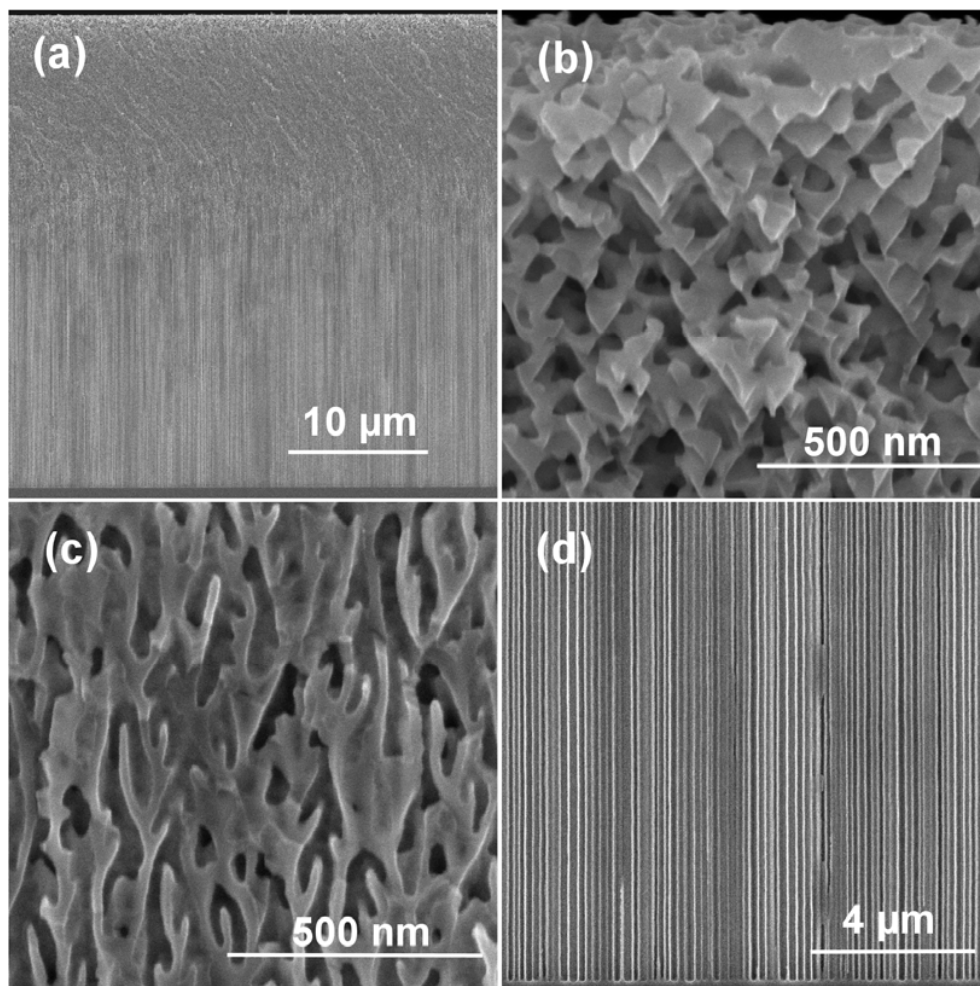
Figure 2. Cross-sectional SEM micrographs of the (011) plane of an n-InP electrode subjected to an LPS from 0 to 3.3 V (SCE) at 25 mV s^{-1} in 4 mol dm^{-3} KCl. Image (a) shows the full thickness (33 µm) of the porous layer, image (b) is of the region of the porous layer near the electrode surface, image (c) is of from a depth of 14 µm into the porous layer and image (d) is taken near the porous/bulk InP interface.

Figure 4 shows SEM images of the samples anodized at a constant potential as in Fig. 3. Figure 4 (a) shows the sample anodized at 1.0 V. A CO pore structure is seen throughout the entire thickness of the layer. The pores appear to be growing along the <111>A directions. The upper part of the layer is fragmented, and this, combined with the relatively shallow layer thickness (~2 µm) in comparison with the amount of charge passed (measured to be 31.5 C cm^{-2} from integration of the curve in Fig. 3) through the electrode indicates that the majority of the surface of the sample was removed *in situ*. This may have been due to the effect of chemical etching (caused by anodically formed intermediates confined within the porous network) or the build-up of stress in the porous structure. The faceted pore walls which are seen for the porous etching of InP in KCl are an indication that some chemical etching is taking place (15, 24). It can also be seen that the pores growing at the very bottom of the layer show a more clearly defined structure and growth direction. However, closer to the surface, the pore structure appears

fragmented and individual pores become difficult to distinguish. This fragmentation is another indication that chemical etching is taking place at the pore walls after the pore tip has progressed beyond them.
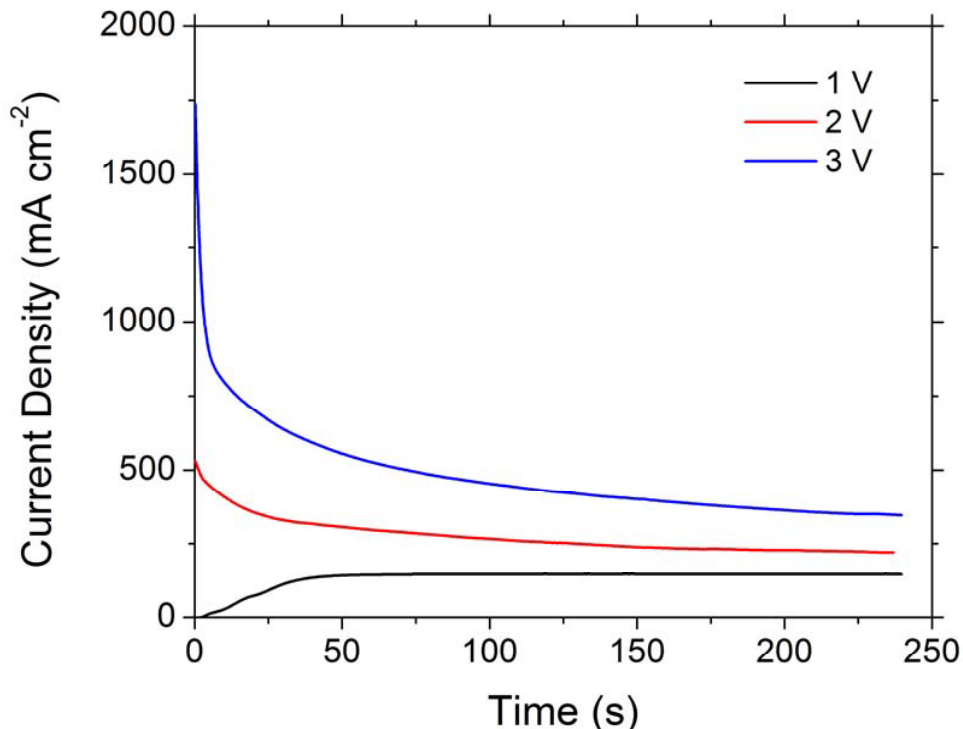

Figure 3. Plot of current density against time for three n-InP electrodes, each anodized at a constant potential between 1.0 and 3.0 V (SCE) for 4 minutes in 4 mol dm^{-3} KCl.

A much thicker layer (~63 μm) is observed in the case of the sample anodized at 2.0 V. This layer shows a brief section of partially CO etching before transitioning into a CLO pore structure, which is shown in Fig. 4 (b). This sample showed a much more planar surface indicating that the majority of the initial electrode surface remained intact. The morphology of the sample anodized at 3.0 V was similar to what was seen for the sample anodized at 2.0 V. However, the porous layer reached a thickness of ~92 μm, corresponding to the highest average etch rate of all samples at 0.38 μm s^{-1}. This is comparable with typical etch rates reported for pore formation in HCl (25-26). At 4.0 V and above, no porous layer was observed indicating that non-porous etching may have taken place.
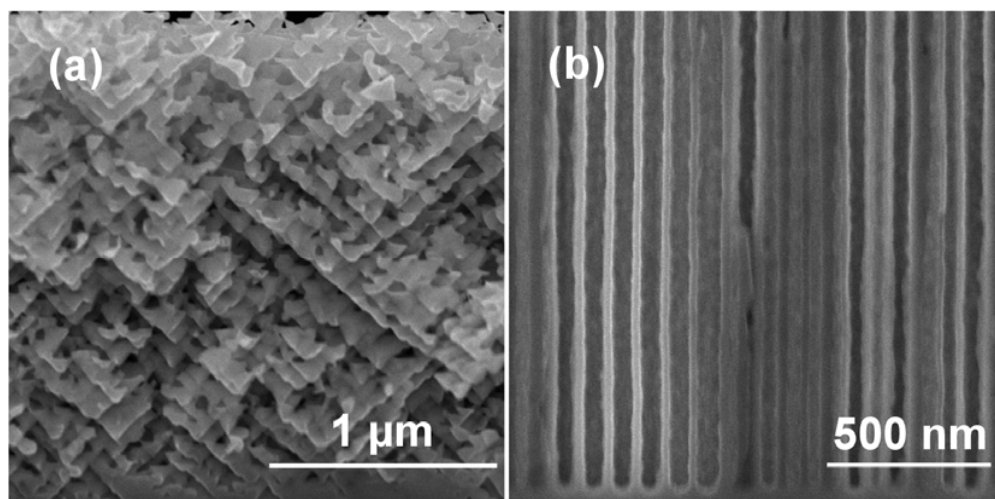
Figure 4. Cross sectional SEM micrographs of the (011) plane of porous layers grown at a constant potential of (a) 1.0 V and (b) 2.0 V in 4 mol dm^{-3} KCl for 4 minutes.

The apparent chemical etching that was seen for the sample anodized at 1.0 V was not observed for the samples anodized at higher potentials. This may indicate the role of chemical intermediates or etch products trapped within the porous structure. The CO structure may act to confine the products of the etch more effectively then the CLO structure due to the more complex nature of the CO pore network, which presents a less direct path for products diffusing out to the bulk electrolyte. Evidence for this may be seen in the current-time plots shown in Fig. 3. As mentioned before, the plots for the samples anodized at 2.0 and 3.0 V show behaviour characteristic of instantaneous nucleation *i.e.* a high density of etch pits was instantly formed on the surface. This would quickly lead to a very densely packed pore structure with a majority of pores connected back to the surface through their own surface pit. The plot for the sample anodized at 1 V however, is characteristic of a gradual nucleation process. This suggests that surface pitting occurred much more gradually and in fewer locations. Such a mechanism would result in a lower spatial density of heavily branched porous domains and since each domain is linked to the surface and thus the electrolyte by a single pit, a reduction in the number of direct porous layer-to-surface pathways. This mass transport bottleneck, along with the more tortuous geometry of the CO pore structure, could lead to a significant reduction in the ability of the growing domains and resulting porous layer to rid itself of reaction intermediates and products. It may be that the more confined etch products are what leads to the significant chemical etching that is seen at lower potentials.

An SEM micrograph of the (100) surface of the sample anodized at 3.0 V for 4 minutes is shown in Fig. 5 (a). Much of the initial InP surface appears to be intact but it is regularly penetrated by a high density of surface pits (~200 µm^{-2}). These surface pits are said to form at defect sites on the surface (22), and result in the formation of porous domains below the surface (16). Figure 5 (b) is an SEM micrograph of the (100) surface of a porous layer formed at 3.0 V but with an etch time that was increased by a factor of three, resulting in a total etch time of 12 minutes. This layer showed CLO pores over its entire thickness, with no visible CO 'nucleation layer'. However, the electrode surface appeared very rough, and the porous layer thickness (~170 µm) was much less than would be expected for a layer etched for 12 minutes based on the amount of charge

passed through the electrode. The layer etched for 4 minutes showed a charge efficiency of 1.37 μm C^{-1} cm^2 (126 C cm^{-2} passed to obtain 92 μm porous layer) while the layer etched for 12 minutes showed a charge efficiency of 1.68 μm C^{-1} cm^2 (285 C cm^{-2} passed to obtain 170 μm porous layer). Assuming no significant variation in charge efficiency occurs as the porous layer thickens, the layer etched for 12 minutes would be expected to be ~38 μm thicker. This indicates that the top section of the porous layer was removed, either during the etch, or during preparation for SEM analysis. This allowed the CLO pore cross section to be viewed on the newly revealed (100) surface which is shown in Fig. 5 (b). A square shaped pore cross section was observed, with the pore walls defined by the {001} planes. It is possible that some KCl deposits were left on the pore walls and that its characteristic cubic structure is what is being observed. However, no contrast difference is seen around the pore walls on SEM images taken at a higher magnification. CLO pores formed in both HCl (5) and KOH (27) typically show rounded cross sections. These square pore cross-sections, can only be produced in HCl electrolytes by the use of additives (19) or by a post processing cathodic decomposition step (28). The average length of the sides of the square was 47 nm and the average pore wall thickness was 20 nm. Pore widths are typically measured on the (011) plane which means that the diagonal of the square would be the measured pore width. Estimates from these measurements give a mean pore width of ~66 nm, which is a typical pore width for CLO pores at a depth of about 40 μm which aligns with the previous estimate of the thickness of the porous layer which had been removed from the electrode surface.
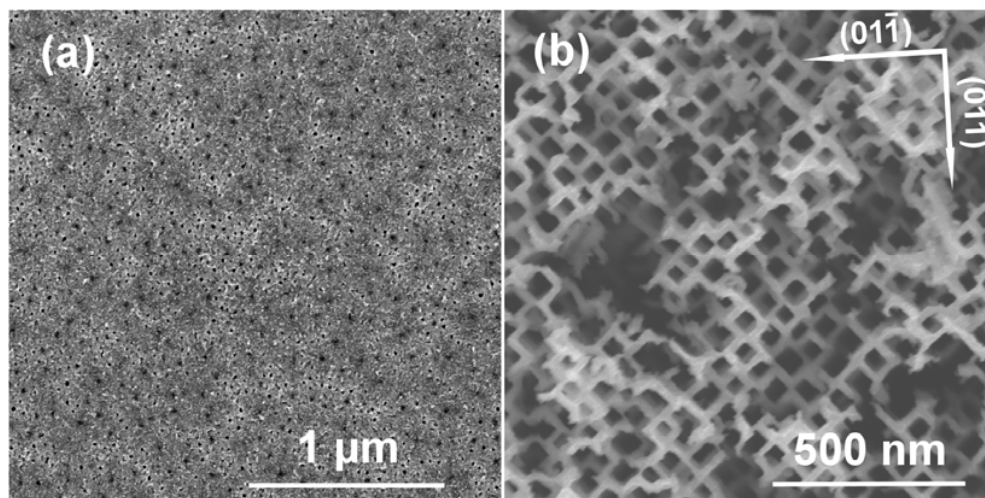

Figure 5. SEM micrographs of the (100) plane of porous layers grown at a constant potential of 3.0 V in 4 mol dm^{-3} KCl for (a) 4 minutes and (b) 12 minutes. Image (a) is of the electrode surface, and image (b) is of a sub surface region (the original surface was removed allowing a view of the CLO pore cross section). The inset shows the crystallographic directions.

Given the relatively ordered nature of the CLO pore structure seen on the (100) plane, it is relatively simple to estimate both the pore density (number of pores passing through the (100) plane) and the porosity for CLO pores at a depth of ~38 μm. Using the measurements of pore width and pore wall thickness from the previous paragraph and assuming a uniform pore distribution, a pore density of 2.2×10^{10} cm^{-2} and a porosity of 49% were calculated.

The average porosity of a porous layer formed in 4 mol dm^{-3} KCl can also be calculated by comparing the porous layer thickness to charge ratio (d_p/Q_p) with that predicted by Faraday's law for the planar etching of InP (d/Q), calculated using Eqn. 1.

$$\frac{d}{Q} = \frac{V_{m(InP)}}{nF} \tag{1}$$

where V_m is the molar volume of InP (30.31 cm^3 mol^{-1}), F is the Faraday constant and n is the number of charge carriers (holes) involved in the electrochemical reaction. Assuming an 8-hole process occurs (as has been reported for the formation of porous InP in other electrolytes (14, 29)) with a reaction (as proposed by Weng *et al.* (14)) of the form

$$InP + 3H_2O + 8h^+ \rightarrow 1/3In(PO_3)_3 + 2/3In^{3+} + 6H^+ \tag{2}$$
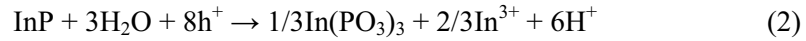
then a porosity of 53% for a layer grown to 92 µm, is calculated. Of course, the porosity may vary with porous layer thickness, and we have observed a variation in porosity as the pore morphology changes form CO to CLO. The 49% porosity that was estimated earlier from the (100) CLO pore cross section seems reasonable considering that it came from a depth of ~38 µm into the porous layer and that the average porosity of a 92 µm layer is 53%. This also indicates that the assumption of an 8-hole process is valid, as a 6-hole process would predict porosities that are much higher than that estimated from the pore morphology at a depth of ~38 µm. The fact that both the porosity and the pore width that were measured on the fragmented (100) surface (Fig. 5 (b)) match the values measured by other techniques, indicates that the pore cross section that was observed is intact, is composed entirely of InP and has not been chemically etched

Galvanostatic Etching of Porous Layers in KCl

The formation of porous layers in KCl at a constant current was also investigated. A plot of potential against time for a sample galvanostatically anodized in 4 mol dm^{-3} KCl at 200 mA cm^{-2} for 15 minutes is shown in Fig. 6 (a). Region I and region II have been marked on the plot. In region I, after a brief initial decay in current, the current begins to increase gradually followed by a much more rapid increase after 200 s. In region II the potential is found to oscillate rapidly. The inset in Fig. 6 (a) shows the potential oscillations between 450 s and 455 s in more detail. Figure 6 (b) shows the amplitude of the Fourier transform of the full potential-time response in (a). It can be seen that the oscillations occurred consistently at around 1.3 Hz. The spread in the frequency spectrum is likely due to the rate of data acquisition being out of phase with the oscillation in potential. Oscillations of both the potential and the current during the formation of porous InP have been observed before in other electrolytes (30-32).
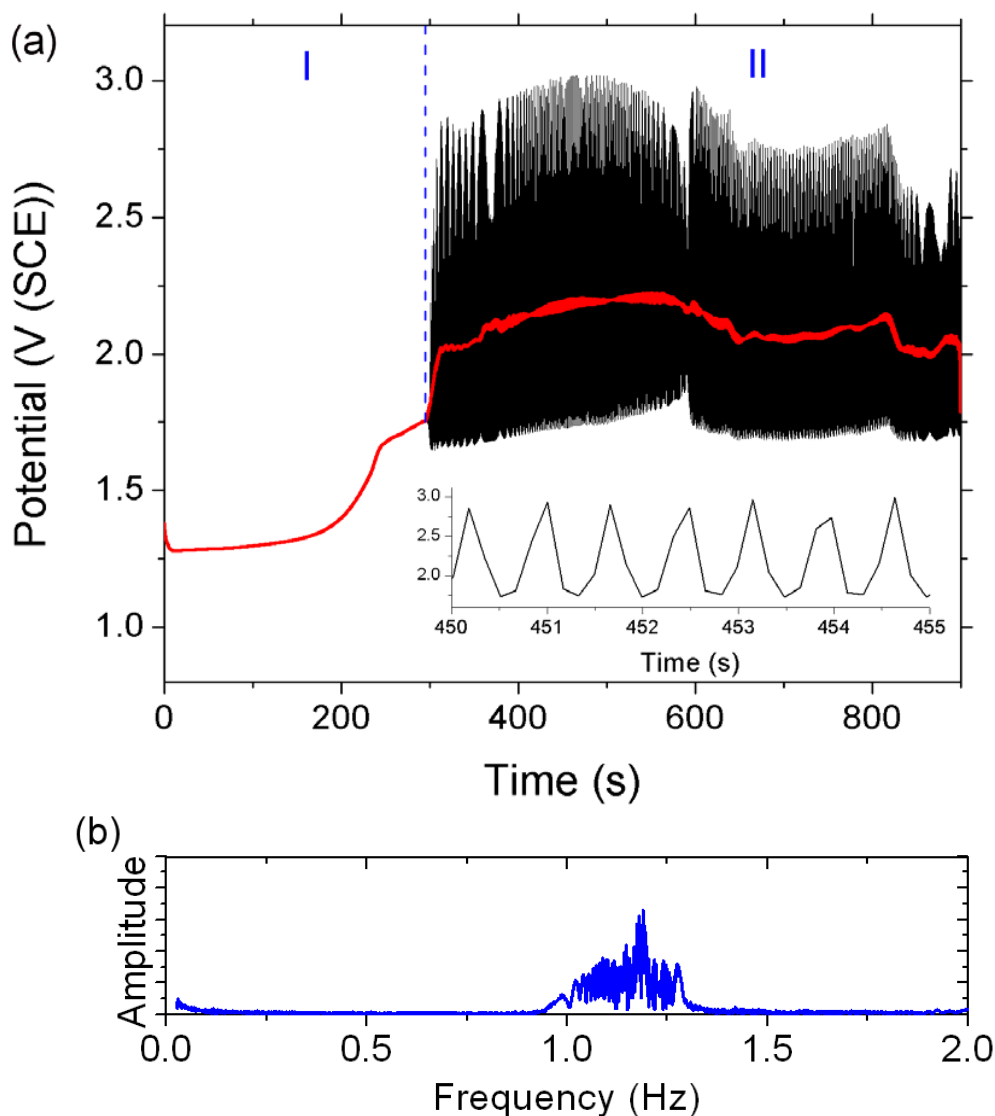
Figure 6. (a) Plot of potential against time for a sample anodized at a constant current density of 200 mA cm^{-2} for 15 minutes in 4 mol dm^{-3} KCl. Regions I, and II are marked. The black line is the measured variation of the potential and the red line is a moving average of the potential data (taken over 50 data points). The inset shows the form of the potential oscillations, magnified from the data in (a) between 450 s and 455 s. (b) Amplitude of the Fourier transform of the full potential-time response from (a) showing a narrow band of oscillation frequencies in the range 1.0 – 1.3 Hz.

Figure 7 shows a series of SEM micrographs of the porous structure that resulted from the galvanostatic etch shown in Fig. 6. Figure 7 (a) shows the entire porous layer grown to a depth of 130 μm. Again, after a period of CO growth, the pores became CLO and remained that way for the duration of the etch. Figure 7 (b) shows a cross section of the electrode surface. The initial ~200 nm of the layer appears much more highly porous than that of the sample anodized potentiostatically. This can also be seen by looking at Fig. 7 (c) which is an image of the (100) surface. In contrast to the relatively smooth surface,

periodically penetrated by pits, that was seen for the potentiostatically etched sample, a highly porous surface was observed for the galvanostatic sample, with no trace of the original InP surface seen. This may simply be due to the large initial value of potential that would have been needed to drive such a large current through the electrode. This would have led to rapid and widespread pit nucleation across the entire sample surface. It may also be that some chemical etching had begun to remove the upper few nm of the porous layer, due to the long etch time (15 minutes) and the resulting increase in exposure to the electrolyte.

Figure 7 (d) is an SEM micrograph of a cross-section of the CLO section of the porous layer near the porous/bulk interface. The pore width can be seen to oscillate, and these oscillations appear to be correlated with the oscillations in potential which were shown in Fig. 5. This was determined by measuring the period of the oscillations (0.73 s) as a fraction of the total time span over which the potential was seen to oscillate (594 s). This was compared with the average distance between pore width maxima and minima in SEM images (80 nm) as a fraction of the total thickness of the porous layer over which the pore diameters were seen to oscillate (68 μm). The two numbers were in good agreement with a ratio of 1.23×10^{-3} calculated for the temporal analysis and a ratio of 1.18×10^{-3} calculated for the spatial analysis. The correlation of pore width oscillations and potential oscillations has been reported before for the porous etching of InP in HCl (30). Pore widths, porosities and charge efficiencies did not vary significantly from those measured during the potentiostatic etches.

Effect of KCl Concentration on Porous Layer Formation

Figure 8 shows a series of LSVs of samples anodized in KCl concentrations varying from 1 mol dm^{-3} to 4 mol dm^{-3}. Both the potential for pore formation (i.e. the potential at which a significant increase in current is observed) and the potential of the first current peak decrease as the KCl concentration is increased. Anodization in 1 mol dm^{-3} KCl resulted in non-porous etching and a very uneven electrode surface. Anodization at all other concentrations resulted in the formation of typical porous layers which transitioned from an initially CO morphology into a CLO morphology as the potential was made more anodic.

Figure 9 shows a series of SEM images of the CLO pores that were formed by anodization of samples in KCl concentrations of 2, 3 and 4 mol dm^{-3} as in Fig. 8. At 2 mol dm^{-3} the pore walls have a very wavy appearance (Fig. 9 (a)) i.e. the pore width appears to oscillate as the porous layer thickens. Such pore width oscillations, which in this case are unaccompanied by oscillations in the current or potential, have been observed before in InP (14). The CLO pores formed in 3 mol dm^{-3} (Fig. 9 (b)) also show pore width oscillations, but to a lesser extent than those formed in 2 mol dm^{-3}. The sample anodized in 4 mol dm^{-3} however, showed very smooth CLO pore walls and no significant pore width oscillations were observed. This indicates that the most uniform pores, and therefore those most suitable for applications which require a high level of structural uniformity (e.g. optical crystals), are formed at 4 mol dm^{-3}.
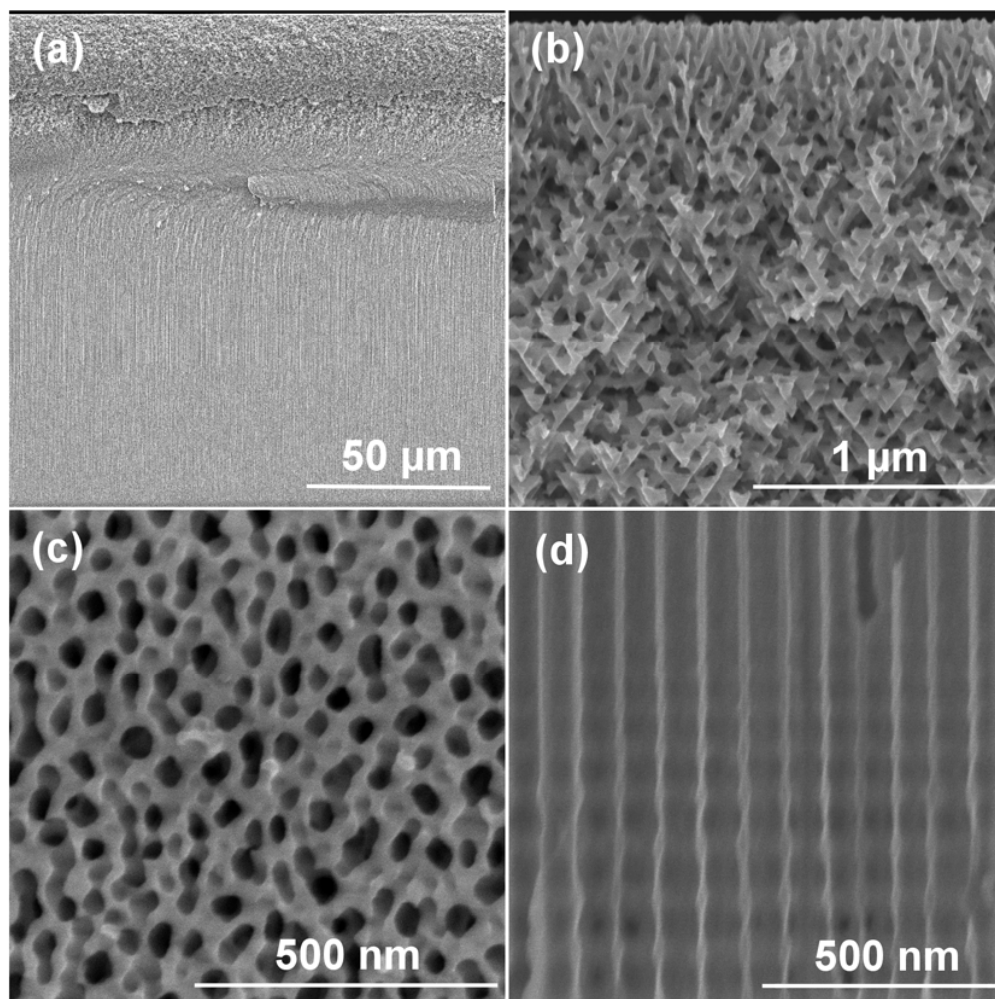
Figure 7. SEM micrographs of an n-InP electrode etched at a constant current of 200 mA cm^{-2} in 4 mol dm^{-3} KCl. Images(a), (b) and (d) are of the (011) cross section and image (c) is of the (100) surface. Image (a) shows the full thickness (130 μm) of the porous layer, image (b) is of the region of the porous layer near the electrode surface, image (c) shows the highly porous (100) surface and image (d) was taken at a depth of ~100 μm and shows CLO pore diameter oscillations.

The pore width oscillations seen at lower concentrations may be understood as a natural part of equilibrium pore etching. We have recently proposed a model for pore formation in which charge transfer between the semiconductor and the electrolyte is seen as a three-step process (24, 27, 33). The first step is hole supply to the semiconductor surface, and this is said to occur preferentially at the pore tips due to the electric-field enhancement provided by the surface curvature as in the model proposed by Zhang (7). Once a hole has arrived at the electrode surface, it may diffuse through the valence band and surface states (step two) until it interacts with the active species in solution and is annihilated in the electrochemical reaction (step three). The spatial extent of etching in the vicinity of the pore tip (or the pore width) is then controlled by both the width of the region of enhanced hole supply at the pore tip and the extra distance over which the holes can diffuse.
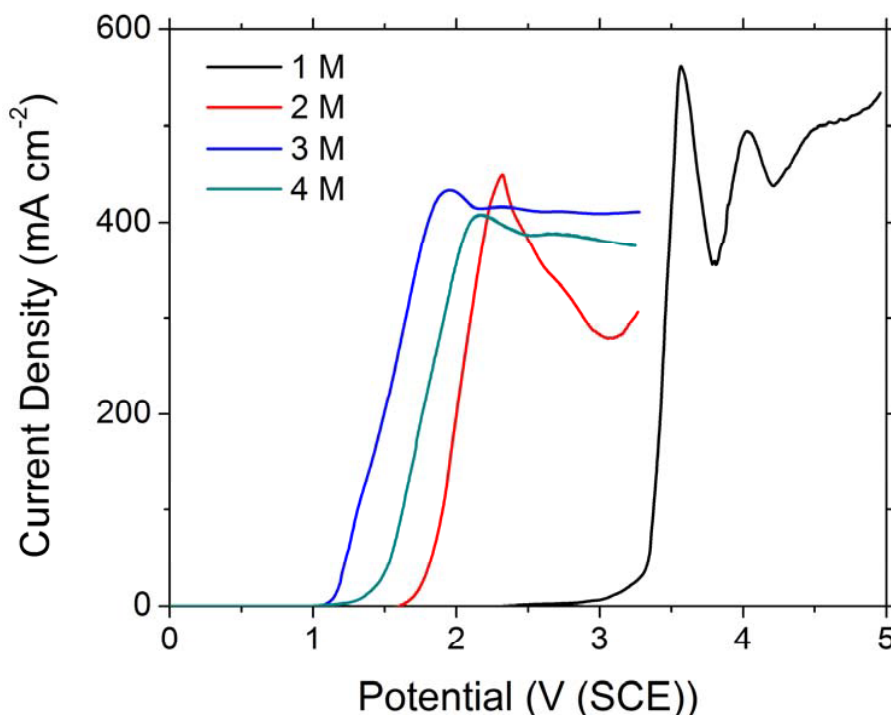
Figure 8. A series of LSVs of n-InP electrodes subjected to a potential sweep at a rate of 25 mV s^{-1} in a range of KCl concentrations. The samples anodized in 1, 2 and 3 mol dm^{-3} had their potential swept between 0 and 3.3 V and the sample anodized in 4 mol dm^{-3} had its potential swept to 4.9 V.

These two factors controlling pore width can interact through a feedback mechanism which may result in oscillation. For example, consider a pore whose width, and therefore, radius of curvature has been defined both by the supply of holes to the pore tip (step one) and by the diffusion of holes from the pore tip (step two). As the etch progresses, the pore may widen slightly as a result of a change in the composition of the electrolyte in the vicinity of the pore tip (affecting step 2), or a change in the distribution of defects or holes in the semiconductor (affecting step 1), possibly due to the presence of a neighbouring pore. However, the wider pore bottom would now have a larger radius of curvature which would reduce the width of the region of enhanced hole supply, leading to pore thinning. Once the pore has thinned, the radius of curvature of the tip would again have decreased leading to more pore widening. This mechanism could then continue indefinitely leading to continuous pore width oscillation. This mechanism would also explain the decrease in pore width oscillation seen as KCl concentration is increased. If the kinetics of the electrochemical reaction increase with concentration, then the effect of hole diffusion on pore width would be expected to decrease as less and less pore widening could be ascribed to this process. This mechanism would also result in the observation of thinner pores at higher concentrations. The average width of the CLO pores was observed to decrease as the concentration increased. The pore width decreased from 99 nm in 2 mol dm^{-3} to 71 nm in 4 mol dm^{-3} and this is shown in Fig. 10. This same trend is observed for porous layers formed in InP in KOH (33) and in Si in HF (34). The magnitudes of the error bars in Fig. 10 are equal to plus and minus one standard deviation

of the layer depth measurements at each concentration. The increased error in the measurements taken at lower KCl concentrations is due to the uncertainty introduced to the measurement by the oscillation of pore width that is seen in these samples.
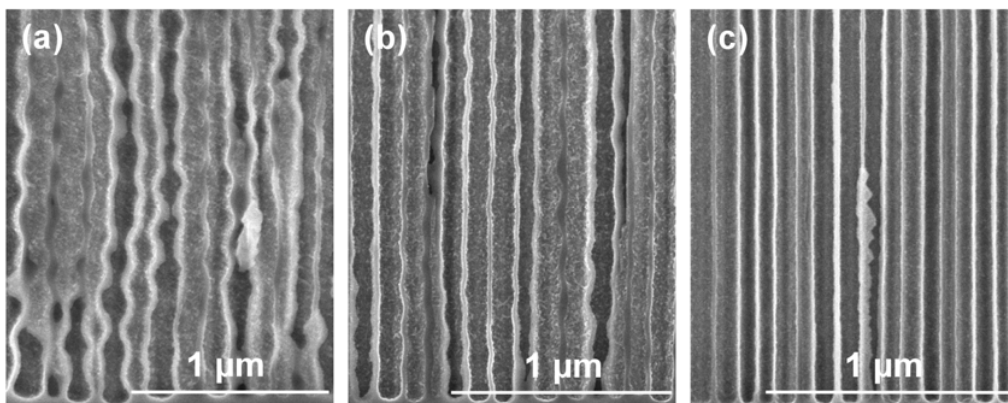

Figure 9. Cross sectional SEM micrographs of n-InP electrodes formed by LPS from 0 to 3.3 V at 25 mV s^{-1} in (a) 2 mol dm^{-3}, (b) 3 mol dm^{-3} and (c) 4 mol dm^{-3} KCl. The images are of the CLO pores formed near the porous/bulk InP interface.
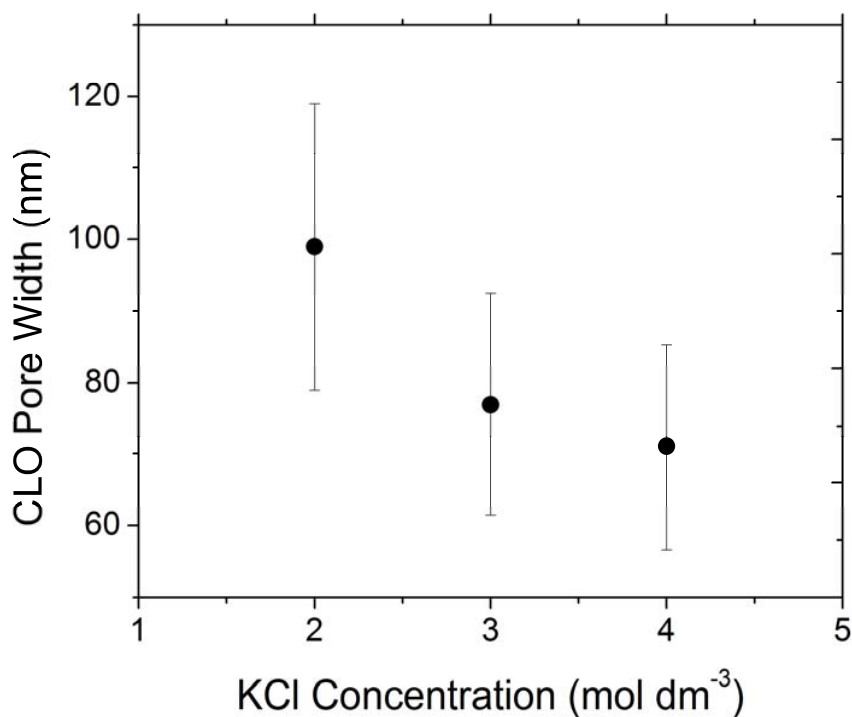

Figure 10. Plot of average CLO pore width against KCl concentration. The error bars are given by one standard deviation of the pore width measurements at each concentration. The larger error seen at lower concentrations is due to the oscillating pore width.

Conclusions

The etching of deep porous layers in InP in KCl solutions with concentrations between 2 and 4 mol dm^{-3} was demonstrated. These layers show a typical porosity of ~50%, can be readily grown to depths of over 200 μm, form 2 distinct pore morphologies over a wide range of potentials, exhibit crystallographically bounded pore walls and show typical etch rates in excess of 0.3 μm s^{-1}.

The role that confined etch products may play in the chemical etching of the porous structure was suggested by the increased amount of chemical etching seen in the more tortuous CO pore network. The gradual nucleation of etch pits also indicated that a greater mass transport workload is placed on surface pits that are formed on electrodes etched at lower potentials.

When formed at a constant current, potential oscillations are observed which have been correlated to oscillations in the pore width. The pores formed at lower concentrations also showed pore width oscillations, but these were not accompanied by a corresponding oscillation in the potential. These oscillations in pore width were explained in terms of a feedback mechanism which can occur if the pore width is controlled by a combination of the effects of the curvature of the pore tip and the lifetime of holes at the pore tip, as proposed in the three-step charge transfer mechanism.

Anodization was attempted at different KCl concentrations in the range 1-4 mol dm^{-3}. Higher concentration electrolytes generally resulted in greater pore uniformity, which is demonstrated by the square CLO pore cross section and smooth pore walls. Average pore width was also observed to decrease as KCl concentration was increased. Combining this uniform pore cross section with surface pre-patterning should allow for the creation of ordered three-dimensional structures with the possibility of photonic applications. Interestingly, porous structures formed in KCl compare favorably to those formed in HCl or KOH electrolytes, but in an electrolyte which is much safer to use.

Acknowledgements

References

1. R. L. Smith and S. D. Collins, *J. Appl. Phys.*, **71**, R1 (1992).
2. L. T. Canham, *Appl. Phys. Lett.*, **57**, 1046 (1990).
3. H. Föll, *Appl. Phys. A-Mater.*, **53**, 8 (1991).
4. M. I. J. Beale, J. D. Benjamin, M. J. Uren, N. G. Chew and A. G. Cullis, *J. Cryst. Growth*, **73**, 622 (1985).
5. H. Föll, J. Carstensen, S. Langa, M. Christophersen and I. M. Tiginyanu, *Phys. Stat. Sol. A*, **197**, 61 (2003).
6. H. Foll, J. Cartensen and S. Frey, *J. Nanomater.*, 1 (2006).
7. X. G. Zhang, *J. Electrochem. Soc.*, **151**, C69 (2004).

8. C. O'Dwyer, D. N. Buckley, D. Sutton and S. B. Newcomb, *J. Electrochem. Soc.*, **153**, G1039 (2006).
9. P. Schmuki, J. Fraser, C. M. Vitus, M. J. Graham and H. S. Isaacs, *J. Electrochem. Soc.*, **143**, 3316 (1996).
10. R. P. Lynch, C. O'Dwyer, D. N. Buckley, D. Sutton and S. Newcomb, *ECS Trans.*, **2**, 131 (2006).
11. M. Christophersen, J. Carstensen, A. Feuerhake and H. Föll, *Mat. Sci. Eng. B-Solid*, **69-70**, 194 (2000).
12. S. Ronnebeck, J. Carstensen, S. Ottow and H. Foll, *Electrochem. Solid-State Lett.*, **2**, 126 (1999).
13. P. Schmuki, L. E. Erickson, D. J. Lockwood, J. W. Fraser, G. Champion and H. J. Labbe, *Appl. Phys. Lett.*, **72**, 1039 (1998).
14. Z. Weng, A. Liu, Y. Sang, J. Zhang, Z. Hu, Y. Liu and W. Liu, *J. Porous Mater.*, **16**, 707 (2009).
15. E. Spiecker, M. Rudel, W. Jäger, M. Leisner and H. Föll, *Phys. Stat. Sol. A*, **202**, 2843 (2005).
16. R. P. Lynch, C. O'Dwyer, D. Sutton, S. B. Newcomb and D. N. Buckley, *ECS Trans.*, **6**, 355 (2007).
17. A. Hamamatsu, C. Kaneshiro, H. Fujikura and H. Hasegawa, *J. Electroanal. Chem.,* **473**, 223 (1999).
18. S. Langa, I. M. Tiginyanu, J. Carstensen, M. Christophersen and H. Foll, *Electrochem. Solid-State Lett.*, **3**, 514 (2000).
19. H. Fujikura, A. Liu, A. Hamamatsu, T. Sato and H. Hasegawa, *Jpn. J. Appl. Phys.*, **39**, 4616 (2000).
20. H. Tsuchiya, M. Hueppe, T. Djenizian and P. Schmuki, *Surf. Sci.*, **547**, 268 (2003).
21. S. Langa, S. Lölkes, J. Carstensen, M. Hermann, G. Böttger, I. M. Tiginyanu and H. Föll, *Phys. Stat. Sol. C*, **2**, 3253 (2005).
22. P. Schmuki, U. Schlierf, T. Herrmann and G. Champion, *Electrochim. Acta*, **48**, 1301 (2003).
23. P. Schmuki, L. Santinacci, T. Djenizian and D. J. Lockwood, *Phys. Stat. Sol. A*, **182**, 51 (2000).
24. R. P. Lynch, N. Quill, C. O'Dwyer and D. N. Buckley, *ECS Trans.*, *this volume* (2012).
25. A. Liu and C. Duan, *Physica E*, **9**, 723 (2001).
26. H. Föll, S. Langa, J. Carstensen, M. Christophersen and I. M. Tiginyanu, *Adv. Mater.*, **15**, 183 (2003).
27. N. Quill, R. P. Lynch, C. O'Dwyer and D. N. Buckley, *Proceedings of Pits and Pores 5: A Symposium in Honor of David Lockwood, Honolulu PRiME 2012,* Abtract 2421.
28. T. Sato, T. Fujino, A. Mizohata and T. Hashizume, in *E-MRS Fall Meeting 2007, Symposium B*, Warsaw (2007).
29. L. Santinacci, M. Bouttemy, I. Gerard and A. Etcheberry, *ECS Trans.*, **19**, 313 (2009).
30. S. Langa, J. Carstensen, I. M. Tiginyanu, M. Christophersen and H. Foll, *Electrochem. Solid-State Lett.*, **4**, G50 (2001).
31. D. N. Buckley, C. O'Dwyer, E. Harvey, T. Melly, M. Serantoni, D. Sutton and S. B. Newcomb, in *in Proceedings of the State-of-the-Art Programme on Compound*

Semiconductors XXXVIII and (2) Nitride & Wide Bandgap Semiconductors for Sensors, Photonics, and Electronics IV, p. 43 (2003).

32. C. O'Dwyer, D. N. Buckley and S. B. Newcomb, *Langmuir*, **21**, 8090 (2005).

33. N. Quill, R. P. Lynch, C. O'Dwyer and D. N. Buckley, *Proceedings of Pits and Pores 5: A Symposium in Honor of David Lockwood, Honolulu PRiME 2012,* Abstract 2420.

34. P. Jaguiro, S. La Monica, S. Lazaronk and A. Ferrari, *in Proceedings of Pits and Pores: Formation, Properties and Significance for Advanced Luminescent Materials*, 358 (1997).